LIMNOLOGY
and
OCEANOGRAPHY: METHODS

ASLO

*Limnol. Oceanogr.: Methods* 13, 2015, 746–762

doi: 10.1002/lom3.10063

# Quantifying the distribution and influence of non-uniform bed properties in shallow coastal bays

**Patricia L. Wiberg,* Joel A. Carr, Ilgar Safak, Arachaporn Anutaliya**
Department of Environmental Sciences, University of Virginia, Charlottesville, Virginia

## *Abstract*

Sediment resuspension and related increases in turbidity in shallow coastal bays are strongly controlled by local bed properties. However, knowledge of bed properties in coastal bays is typically sparse at best. In this study, we developed a method to estimate the spatial distribution of bed properties in shallow coastal bays using a combination of bed sediment measurements and residence time calculations that requires neither extensive dedicated modeling nor extensive sampling. We found a strong relationship between water residence times derived from a coastal hydrodynamic model and observed bed grain size fractions in a system of coastal bays and used that relationship to transform maps of residence time to maps of grain size fractions throughout the bays. Because grain-size fractions are related to other bed properties such as organic fraction, permeability and cohesion, these maps provide valuable information for habitat studies as well as morphodynamic modeling. We used our maps of grain size distributions to initialize a 2-month-long model simulation of currents, waves and suspended sediment forced with measured wind and tides. Spatial variations in suspended sediment concentration (SSC) reflected spatial gradients in sand and mud abundance in the bed. Lower SSC in sandier regions of the bays, near barrier islands and inlets, resulted in higher benthic light availability but lower sediment supply for deposition on back-barrier marshes. Higher SSC in more landward, muddier regions resulted in greater light attenuation and sediment availability for deposition on mainland fringing marshes. The proposed methodology facilitates quantification of these bed-dependent spatial variations in SSC.

Geomorphic, ecological, and biogeochemical processes in shallow coastal bays are strongly influenced by the properties of the sediment comprising the bay bottom. For example, water column suspended sediment concentration (SSC) is often used as a proxy for sediment availability for marsh accretion (Kirwan et al. 2010) and also mediates the light available for photosynthesis in benthic plants (Gallegos 1994; Lawson et al. 2007). Values of SSC for given wave and current conditions are controlled by the erodibility and settling rates of bed sediment, which in turn are functions of the bed sediment grain size distribution. Furthermore, many bed properties that affect benthic plants and animals are tied to sediment grain size, including organic matter fraction and permeability (Fonseca and Bell 1998; Koch 2001).

Despite the sensitivity of SSC, benthic biota, and biogeochemical processes to bed characteristics, knowledge of bed sediment properties in coastal bays is typically limited to analysis of a relatively small number of bed sediment samples. Bed sediment grain size in shallow coastal bays can exhibit strong spatial variations ranging from predominantly sandy beds in higher energy regions closer to oceanic influence, e.g., near barrier islands and inlets, to predominantly muddy beds near the lower energy inland border of a bay (e.g., Lawson et al. 2007). This range encompasses both cohesive and non-cohesive sediment behavior as well as high and low bed permeability. Analysis of a small number of bed samples is unlikely to be sufficient to characterize the spatial heterogeneity of bed sediment in these bays.

Previous investigations of spatial distributions of bed properties in coastal bays have used field sampling and analysis of bed sediment (e.g., Carniello et al. 2012; Law et al. 2013; Fagherazzi et al. 2014) and suspended sediment (Venier et al. 2014), models (van der Wegen et al. 2011a,2011b) and remote sensing (Van der Wal and Herman 2007; Castillo et al. 2011). Field sampling requires many samples to adequately characterize variations in bed sediment in systems exhibiting strong variability, which is often infeasible from the standpoints of both sample collection and sample processing. Correlating sediment properties with more easily measured site parameters such as water depth and distance from an inlet (e.g., Carniello et al. 2012) can facilitate generalization from a limited set of sediment samples. Modeling

*Correspondence: pw3c@virginia.edu

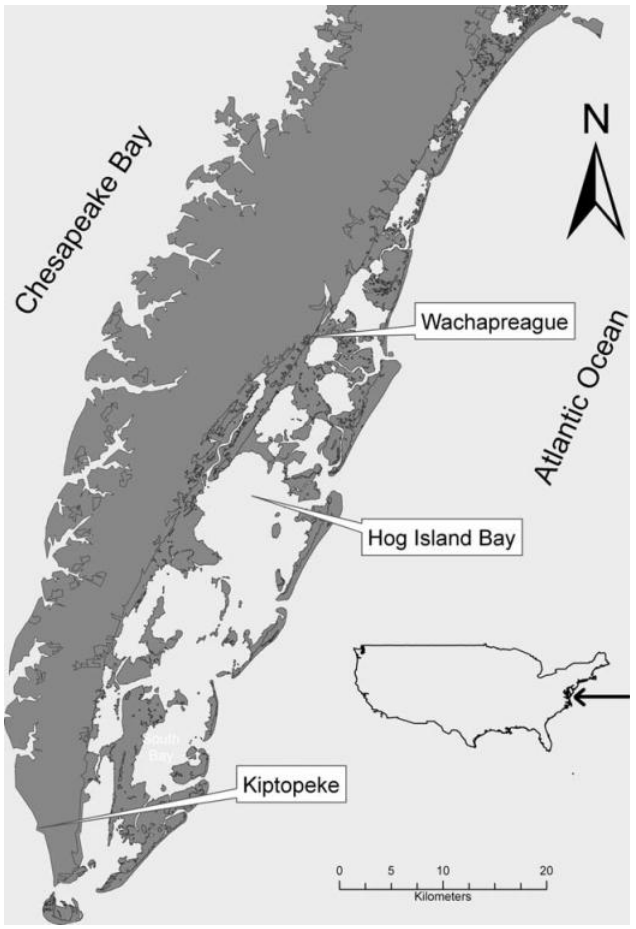


**Fig. 1.** Location map for the southern Delmarva Peninsula, bounded by Chesapeake Bay to the west and the Atlantic Ocean to the east. The Virginia Coast Reserve (VCR) comprises the barrier islands, bays and marshes on the eastern side of the southern (Virginia portion) of the Delmarva Peninsula. Also shown are the locations of Hog Island Bay, a central bay that has been the focus of a number of previous hydrodynamic modeling and measurement studies; Wachapreague, VA, the location of the NOAA tide gauge used in this study; and Kiptopeke, VA, the location of the meteorological station used in this study.

approaches generally involve hydrodynamic redistribution of sediment from an initially uniform, well mixed bed. Under real-time sediment transport conditions, the necessary redistribution could take years of simulation time, although Roelvink (2006) and van der Wegen and Roelvink (2008) show that it is possible to greatly accelerate the rate of adjustment using a morphological factor that amplifies the changes in bed composition at each time step during the adjustment period. Remote sensing methods for estimating sediment properties, which typically involve development of correlations among wavelengths available in the imagery and ground-based measurements (Van der Wal and Herman 2007), may be best suited to intertidal environments.

Here, we describe a new approach to quantifying the spatial distribution of bed sediment size that couples limited field sampling with relatively short duration hydrodynamic model runs to define the spatial distribution of grain size fractions within a system of shallow coastal bays. The approach rests on a hypothesis that bed sediment size is correlated with water residence time, based on the expectation that relatively high-energy portions of coastal bays are close to inlets, have short residence times, and are typically sandy while relatively low-energy portions of bays have longer residence times and finer sediment. This segregation of the bed into sandier and muddier zones is expected in a tidally forced coastal system with time for the bed to equilibrate with the flow conditions. What is new here is the suggestion that residence time is a good proxy for system "energy" and can be used to define the distribution of sediment in coastal bays. The hypothesis is tested in a system of shallow coastal bays on the mid-Atlantic coast of the U.S. We then explore the importance of spatial variations in bed properties on spatial patterns of SSC and consider some implications of these spatial variations.

## Study area

We developed and tested our method for quantifying spatially varying bed sediment grain size distributions in a system of shallow bays on the Atlantic coast of the southern (Virginia) portion of the Delmarva Peninsula (Fig. 1). This system, referred to as the Virginia Coast Reserve (VCR) includes 14 barrier islands sheltering about as many shallow bays of varying size and configuration along with their fringing marshes (Fig. 2a). The mainland side of the system comprises numerous small watersheds, none of which are large enough to supply significant quantities of freshwater or sediment into the system (Olson et al. 2006). Dominant land use in the watersheds is agricultural, but little nitrogen runs off into the bays with the result that water quality in the bays remains very good (Giordano et al. 2011). Average depth of the bays is 1.0 m below mean sea level (Safak et al. 2015) but a number of bays are cut through by deeper channels connected to inlets (Fig. 2a). Most of the bay bottoms are unvegetated, but several bays in the system are currently sites of a large seagrass restoration project designed to restore seagrass to these bays after a system-wide die-off in the 1930s owing to disease and storms (Orth et al. 2006). Sea level along this portion of the coast is rising at a rate of about 4 mm/yr.

A number of previous studies have examined the hydrodynamics of portions of the VCR using field studies and modeling (Lawson et al. 2007; Fagherazzi and Wiberg 2009; Mariotti et al. 2010), including effects of vegetation on flow (Carr et al. 2010; Hansen and Reidenbach 2012). Representative root-mean-squared (RMS) velocities (Fig. 2b; Safak et al. 2015) in response to semi-diurnal tides (tidal range $\sim$ 1.2 m) and typical winter wind conditions (mean wind speed $\sim$ 5.6 m/s) illustrate the generally moderate but

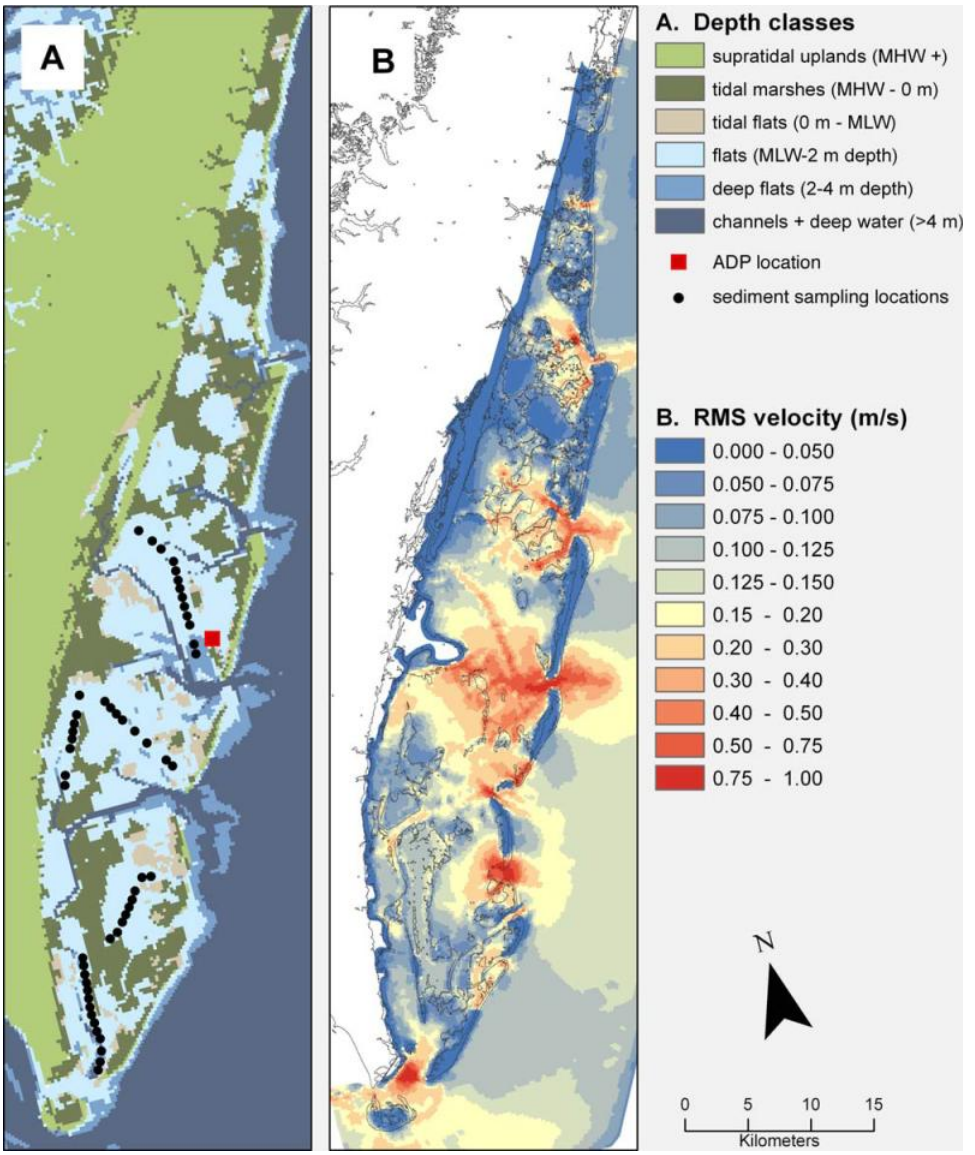


**Fig. 2.** (a) Map of the study area (Virginia Coast Reserve; VCR) on the eastern side of the Delmarva Peninsula in Virginia showing major landscape units. The coastal bays (shown in light blue) are the focus of our study. Black dots show sediment sampling sites along four transects numbered from north to south. The red square is the location of measurements collected with an Acoustic Doppler Profiler (ADP). (b) Root-mean-square (RMS) velocity in the study area determined from a 2-month-long model simulation of wind- and tide-driven circulation in the bays.

spatially varying currents in the bays. Waves that form in response to local winds are depth- and sometimes fetch-limited, depending on wind direction (Fagherazzi and Wiberg 2009; McLoughlin et al. 2015). Waves generated when wind speeds $> 7$ m/s are responsible for the episodically high shear stresses at the bay bottom that are capable of increasing SSC well above background levels (Lawson et al. 2007; Mariotti et al. 2010).

Several studies have related bay hydrodynamics to water and particle residence times in bays in the VCR. Fugate et al. (2006) used Lagrangian particle tracking coupled with a coastal hydrodynamic model to estimate the spatial distribution of residence time in one of the large, central bays of the VCR (Hog Island Bay, Fig. 1). Allen et al. (2011) used remote sensing and in situ tracers to examine residence times in the same bay. Most recently, Safak et al. (2015) used Lagrangian particle tracking in the FVCOM hydrodynamic model (Chen et al. 2006) to characterize the spatial distribution of residence times in a subset of bays in the VCR and proposed a method for estimating residence time for all of the bays in the model domain, described below. Variation in residence time across the bays in the system is a central element of the method we have devised for estimating the spatial distribution of sediment size fractions in these coastal bays.

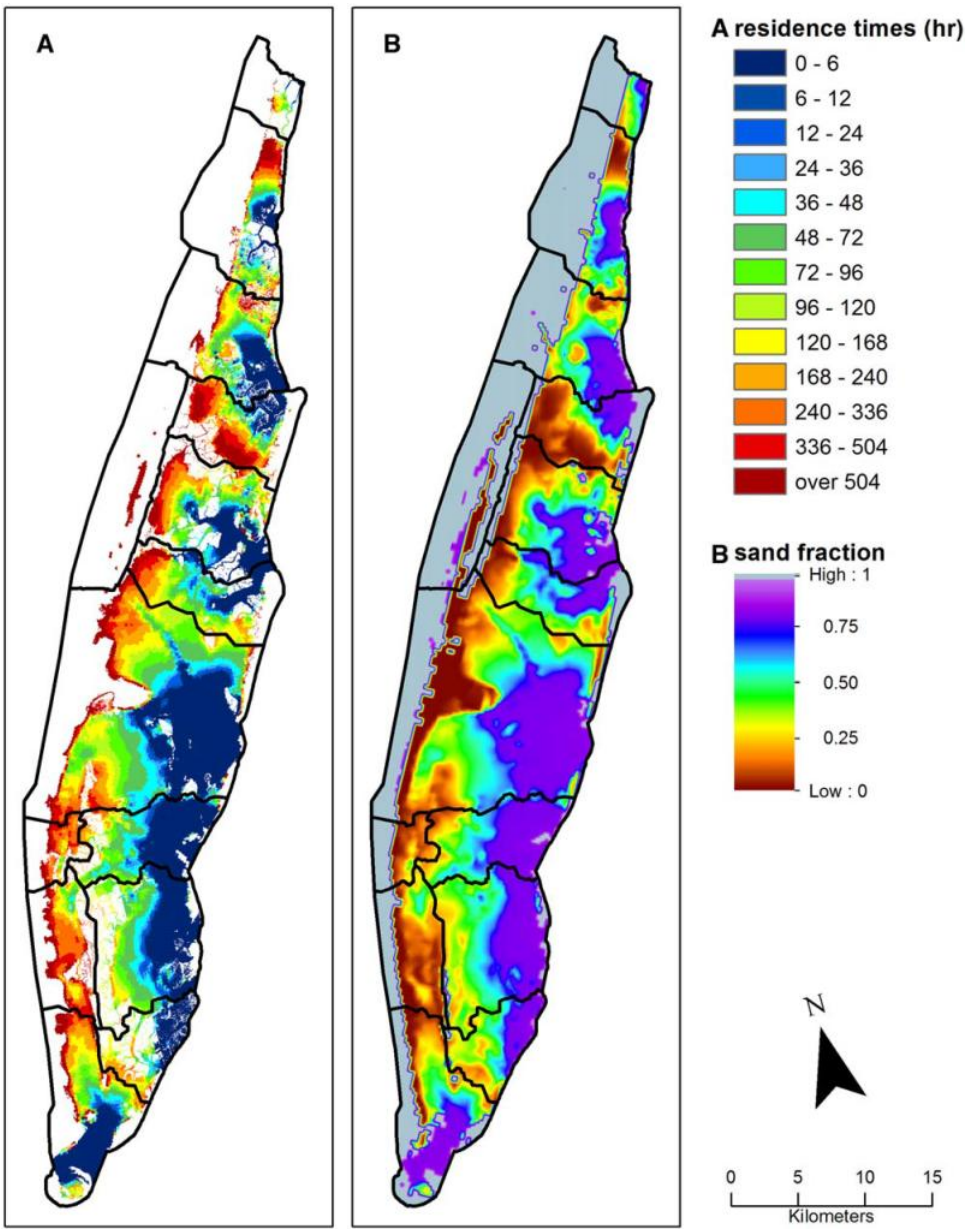


**Fig. 3.** (a) Calculated water residence times in the bays of the study area. (b) Spatial distribution of the sand fraction ($\geq$ 64 $\mu$m) of bed surface sediment estimated from the residence time map in (a) using the relationships we developed between measured grain size fractions and calculated residence times. Regions shaded in gray are supertidal and therefore unaffected by the hydrodynamic simulations presented here.

## Methods

### Sediment sampling and analysis

Four sediment sampling transects (Fig. 2a) were selected to cross strong gradients in residence time (Fig. 3a) in four of the bays in the southern portion of the study area. Bay bottom sediment samples were collected on 07 August 2012–08 August 2012 along the four transects. Samples were collected during periods of mid-high tide using an extendable pole with a plastic syringe tube attached to its end. The pole could only be extended to 3 m, so no samples deeper than 3 m were collected. The uppermost 2 cm of bed sediment from sixty-five sampling sites, approximately evenly spaced along the transects, was analyzed for grain size and organic content.

Organic content was estimated as the difference between the weight of dried samples before and after combustion in a 500°C furnace for more than 6 h. Sediment size was measured using a Beckman Coulter Laser Diffraction Particle Size Analyzer (PSA). Grains $>$ 1 mm were sieved out as required for the PSA; for most sites, 1–2 g of shell material and coarse

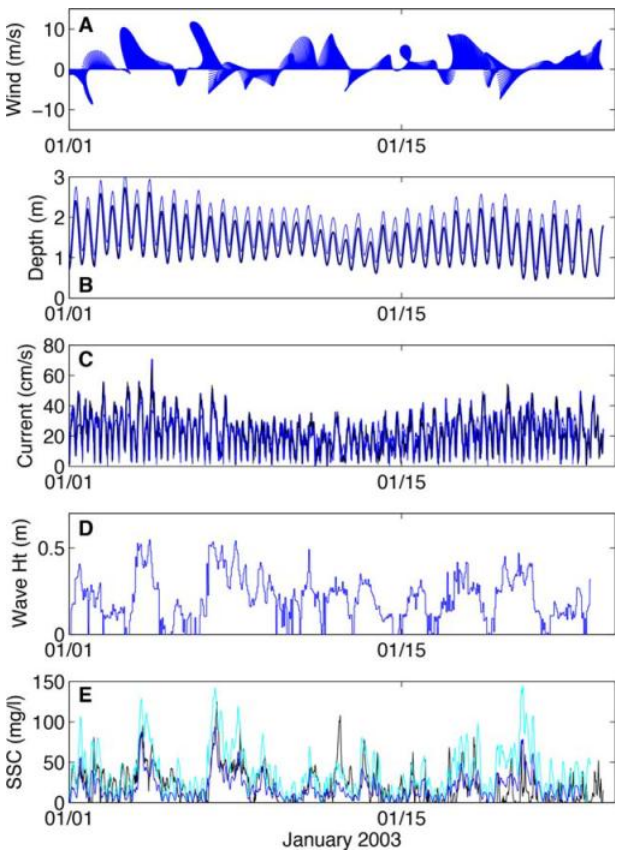


**Fig. 4.** Time series of (a) wind forcing, (b) water depth, (c) currents, (d) significant wave height, and (e) suspended sediment concentration (SSC) during the second month of the simulation period at the deployment site of a current profiler (ADP) in Hog Island Bay (Fig. 2a). Measured (black) and simulated (blue) water levels, currents and SSC are shown for comparison, with SSC for the uniform bed in lighter blue. No useful wave measurements were made during the deployment. The significant wave heights shown in (d) are calculated using the SWAN wave model.

sand was sieved out of the roughly 15 g samples used for grain size analysis. Any visible organic material (e.g., stems or roots) was removed from samples, if present. The remaining organic material was removed by addition of hydrogen peroxide (Law et al. 2013). Sodium hexametaphosphate (0.5 mL) was added to muddy samples to ensure disaggregation of sediment particles. Values for each sample are the average of three replicates.

### Residence times

Residence time for each bed sediment sample location was extracted from the values calculated by Safak et al. (2015) for a number of bays in the Virginia Coast Reserve (VCR) based on tracking of neutrally buoyant tracers in the FVCOM (Chen et al. 2006) hydrodynamic model. Particle tracking residence times (PTRT) were determined for 30 high-tide and 30 low-tide releases of tracers during two 2-month periods of time from 775 locations, including locations within each of the bays where sediment samples were collected; see Safak et al. (2015) for details of the methods used to calculate PTRT. Values used here were averages of high tide releases because these gave the strongest residence time gradients across the bays. However, relationships between grain size and residence time remained significant if residence times were averaged over low-tide releases or all releases.

Because particle tracking residence times were not calculated for all locations in all bays and a goal of our study was to create maps of spatially varying sediment properties for the whole system, we used the method proposed by Safak et al. (2015) to estimate residence times for all of the bays in the model domain. They calculated shortest-path residence time (SPRT) for all points in the model grid as $D/V$ where $D$ is the shortest distance of each point from the closest inlet and $V$ is the RMS velocity at that point. Actual residence times are longer than SPRT for points outside the footprint of the tidally refreshed water volume close to the inlet of each bay because the particles take circuitous routes from their release point to the exit point (an inlet) as they are transported by the tides. Safak et al. (2015) found a relationship between PTRT and SPRT that can be used to convert shortest-path estimates of residence times to estimates of actual residence time over the full set of bays in the VCR (Fig. 3a).

### Hydrodynamic modeling

For this study, we used the Delft3D coastal hydrodynamic and sediment transport model (Roelvink and Van Banning 1994) to calculate flow, waves, and sediment resuspension in the bays of the VCR. The model used a rectangular grid of 107 by 378 nodes with 250 m spacing based on a bathymetric grid updated in 2014 (Richardson et al. 2014). Delft3D was run in coupled mode with the SWAN wave model (Booij et al. 1999) to calculate both depth averaged flow velocities and sediment concentrations.

Simulations focused on a 2-month period in the winter of 2002–2003 when Sontek Acoustic Doppler Profiler (ADP) measurements of flow and SSC (Fig. 4; Lawson et al. 2007) were collected at a site in Hog Island Bay (Fig. 2a). Hourly tidal and wind data were used as drivers for the modeling period December 2002–January 2003 (Fig. 4). Wind forcing for this period was obtained from NOAA's Kiptopeke, VA meteorological station (Fig. 1). We have assumed that winds over the VCR can be approximated as spatially uniform, as was done in previous studies (Mariotti et al. 2010; Safak et al. 2015) and is supported by a good correlation of wind records from different locations in the model domain during some common periods of record (McLoughlin et al. 2015). Tide levels were taken from the NOAA tide gauge at Wachapreague, Virginia (tidesandcurrents.noaa.gov; Fig. 1) and imposed at the model boundaries with the time shift and

amplitude adjustment necessary to reproduce the measured tides.

Delft3D simulations were run for two initial bed configurations. In one, the bed was initially spatially uniform, while in the second, the grain size distribution of the bed varied spatially based on residence times. In both cases, the bed grain size distributions were allowed to evolve over time during the model runs, with bathymetry held constant. Modeled currents and suspended sediment concentrations under the two bed scenarios were compared to measured time series of currents and SSC (Fig. 4).

**Initial bed characterization**

Linear regression was used to evaluate the significance of the relationships between grain size fractions (sand, coarse silt, and finer silt and clay) and residence time. The initial assessment was made using values of particle-tracking residence time (PTRT) from Safak et al. (2015) interpolated to the locations of the sediment samples. We consistently defined the sand fraction as sizes $\geq 64$ $\mu$m, but considered several options for subdividing the mud fraction ($< 64$ $\mu$m) to explore the sensitivity of that choice on the strength of the resulting relationships. Significant relationships between size fractions and PTRT at the 95% confidence level were used to indicate that the approach merited further consideration.

Values of PTRT were not available for all bays in the VCR. Therefore we used the mapping between shortest-path residence time (SPRT) and PTRT developed by Safak et al. (2015) to generate a map of estimated residence time over the full model domain (Fig. 3a). These estimated values were also compared to grain size fractions (and PTRT) to assess their significance and develop relationships to allow us to translate maps of estimated residence time to maps of estimated grain size distributions. These grain size maps were then used to specify initial bed grain size distribution in the spatially non-uniform bed simulations. An initially uniform bed was generated by summing the mass of each size fraction in the spatially non-uniform bed and then using the resulting mass fractions to specify grain size uniformly over the model grid. In this way, the same initial mass of each grain size fraction was present within the modeling domain at the beginning of all simulations.

Initial grain size distributions in the simulations were set to be constant with depth below the bed surface for both the spatially uniform and non-uniform bed cases. Active layer thickness, which only affects the availability of sediment during an individual time step, was set at 5 cm. Bedload and suspended load for non-cohesive fractions in Delft3D are calculated using the formulations of van Rijn (van Rijn 1993; van Rijn et al. 2001). Erosion, $E$, of the cohesive fraction in Delft3D is calculated using the Partheniades-Krone formulation, $E = M(\frac{\tau}{\tau_{cr}} - 1)$ for $\tau > \tau_{cr}$, where $\tau$ is bed shear stress, $\tau_{cr}$ is the critical shear stress (a constant in this formulation), and $M$ (kg m$^{-2}$ s$^{-1}$) is the erosion parameter (Partheniades 1965). The critical shear stresses for erosion was set to 0.04 N m$^{-2}$ (Lawson et al. 2007). To set the value of the erosion parameter in our simulations, $M$ was adjusted by orders of magnitude to arrive at a value of $1 \times 10^{-5}$ kg m$^{-2}$ s$^{-1}$, which minimized the sum-squared error between measured and modeled SSC for both bed approaches. Layer porosity was held constant at 0.70 for all layers regardless of grain size composition. A constant value was necessary to avoid having to change bed porosity as the bed evolved. A porosity of 0.7 is representative of muddy beds but a little high for sandy beds. The sensitivity of the results to this and other model parameters is considered in the Assessment below.

For the sand fraction, a representative median grain diameter for non-cohesive sediment of 125 $\mu$m was specified; Delft3D internally calculates the settling velocity for sand. We used a settling velocity of 3.6 mm s$^{-1}$ for the 32–64 $\mu$m coarse silt fraction and a representative floc settling velocity of 0.75 mm/s for the $< 32$ $\mu$m size fraction, which is in the range of floc settling velocities observed in muddy coastal environments (e.g., French and Spencer 1993; Furukawa et al. 1997; Khelifa and Hill 2006). Studies of suspended particles in tidal creeks and flats (Voulgaris and Meyers 2004; Hill et al. 2013) and of marsh and tidal flat deposition (Christiansen et al. 2000; Law et al. 2013) have identified the important role of flocs in muddy coastal environments like the Virginia coastal bays. The assumption that the $< 32$ $\mu$m fraction settles as flocs causes the water column to clear more quickly than if a significant fraction of the particles remained disaggregated.

## Assessment

**Bed sediment properties**

Grain size varied along the sampling transects in each bay (Fig. 5), with higher sand fractions closer to the inlets and higher mud fractions further from the inlets and closer to the mainland. Sand fractions ($\geq 64$ $\mu$m) were highly correlated with clay fractions ($< 4$ $\mu$m) ($R^2 = 0.96$; Fig. 6a). Clay fractions of 10% or more have been argued to be indicative of cohesive bed behavior (van Ledden et al. 2004). Given the strong correlation between sand and clay fractions in the study area, we can use sand fractions $< 65\%$ as a surrogate for clay fractions $> 10\%$.

Organic fractions are strongly correlated with clay fraction ($R^2 = 0.82$). Again, because of the strong relationship between sand and clay fractions, we also found a significant correlation between sand and organic fraction ($R^2 = 0.84$; Fig. 6b). These relationships allow us to use the spatial distribution of the sand fraction to broadly represent spatial variations in bed cohesiveness and organic fraction as well as grain size and permeability.

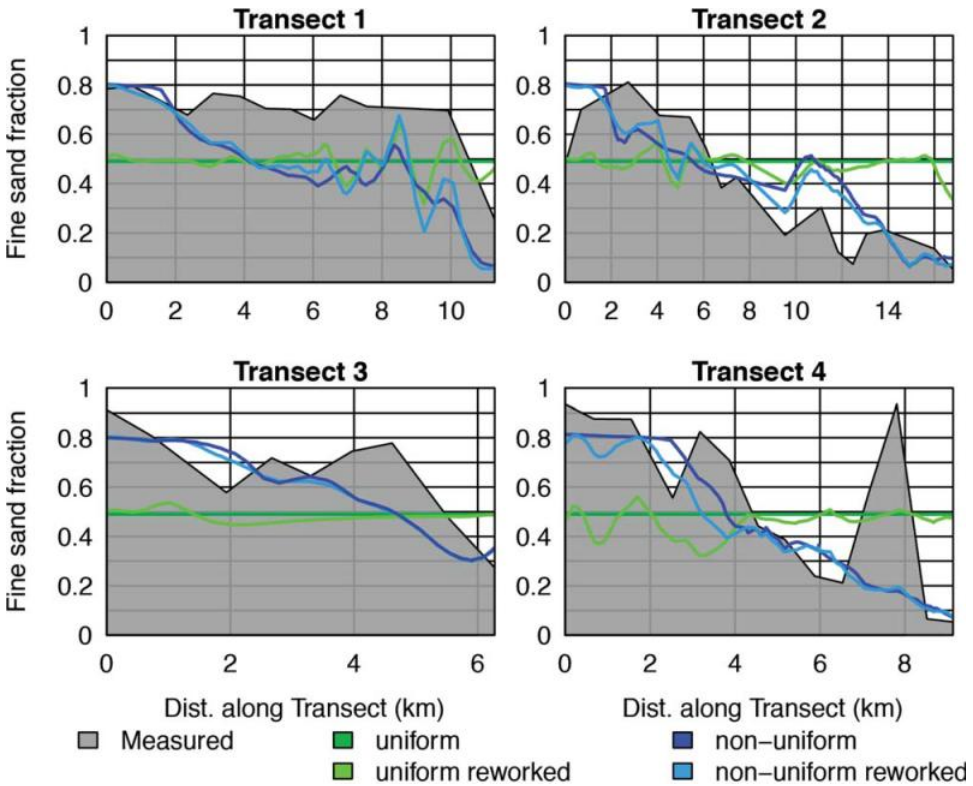


**Fig. 5.** Measured and estimated sand fractions along four sampling transects (Fig. 2a, numbered from north to south). Each transect is plotted with the inlet at the origin. The gray shading indicates measured sand fractions. The blue lines show estimated sand fraction at the beginning (dark blue) and end (light blue) of the 2-month simulation using the initially non-uniform bed. The green lines show beginning (dark green) and end (light green) sand fractions for the initially uniform bed simulation.

**Bed sediment size and residence time**

Scatter plots of measured grain size fractions vs. particle-tracking residence times (PTRT) for the four sampling transects revealed a significant negative relationship between sand fractions and PTRT ($R^2 = 0.55$; Fig. 6c) and a significant positive relationship between $< 32$ $\mu$m silt and clay and PTRT ($R^2 = 0.59$; Fig. 6d). The 32–64 $\mu$m fraction displayed relatively constant percentages ($\sim$ 10%) over all sampling transects, regardless of residence time.

Generally similar relationships were found between measured grain size fractions and the system-wide estimates of residence times shown in Fig. 3a. Grain size data were binned into $< 32$ $\mu$m, 32–64 $\mu$m, and $> 64$ $\mu$m fractions and regressed to obtain simple linear transfer functions for residence time to grain size (Fig. 7; all relationships are significant at the 95% confidence level). The $> 64$ $\mu$m was fit with a piecewise function, linear up to 300 h and constant 10% above 300 h. The 32–64 $\mu$m was fitted with a simple linear regression, whereas the $< 32$ $\mu$m fraction was calculated as the remainder from 100% (green line in Fig. 7c, which is not significantly different than a linear fit to measured values of the $< 32$ $\mu$m fraction). The two-part fit of the $> 64$ $\mu$m was imposed to constrain both the $> 64$ $\mu$m and $< 32$ $\mu$m fractions for high values of residence times.

Given these significant relationships between measured grain size fractions and system-wide estimates of residence times, the spatial map of residence time (Fig. 3a) was used with the regressions shown in Fig. 7 to map the $< 32$ $\mu$m, 32–64 $\mu$m, and $> 64$ $\mu$m size fractions over all bays in the study area. These mappings (e.g., Fig. 3b for the sand fraction) were used to specify the initial mass of each bed fraction for the non-uniform-bed model simulations. Generally, near-inlet regions have higher sand fractions and more distal parts of the bays have low sand (and therefore high mud) content, but relative amounts of sand, coarse silt and finer mud fractions vary from bay to bay (Fig. 3b). Summing over all bays yielded 41% $< 32$ $\mu$m, 10% 32–64 $\mu$m, and 49% $> 64$ $\mu$m. These are the percentages of each size fraction used for all bay bottom grid points in the initially spatially uniform bed.

**Model: data comparison**

Observed and modeled water depths at the ADP site in Hog Island Bay (Fig. 2a) are very highly correlated although the interpolation from the relatively coarse model grid bathymetry to the deployment site resulted in $\sim$ 0.3 m depth discrepancy. Measured and modeled depth-averaged currents at the ADP site have a correlation coefficient of

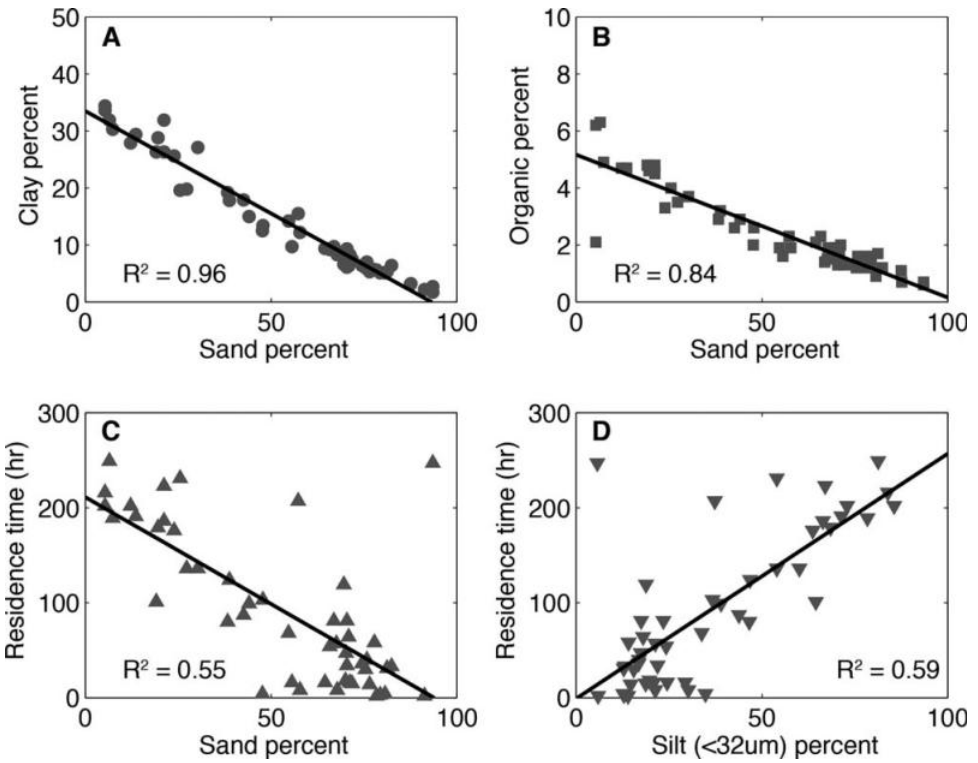


**Fig. 6.** Relationships between (a) measured sand and clay fractions and (b) measured sand and organic fractions for all sediment sampling sites. Relationships between particle-tracking residence times at the sampling locations and (c) measured sand ($\geq$ 64 $\mu$m) content and (d) medium-fine silt and clay ($<$ 32 $\mu$m) content are also shown. All relationships are significant at the 95% confidence level.

0.72. Mean measured and modeled current speeds were almost identical but generally the model tended to underestimate measured peak current velocities ($>$ 30 cm/s) by almost 25%, in part because of the deeper water depth. Reliable measurements of surface wave conditions were not available for the ADP deployment, but other studies have shown that modeled wave conditions in Hog Island Bay (including those calculated with SWAN; Fig. 4d) are typically in good agreement with measured wave conditions (Mariotti et al. 2010; Safak and Wiberg 2012; McLoughlin et al. 2015).

Values of suspended sediment concentration (SSC) for the ADP deployment were obtained by calibrating ADP backscatter with in situ sampling of SSC (Lawson et al. 2007); mean SSC over the full deployment was 28 mg/L. Modeled values

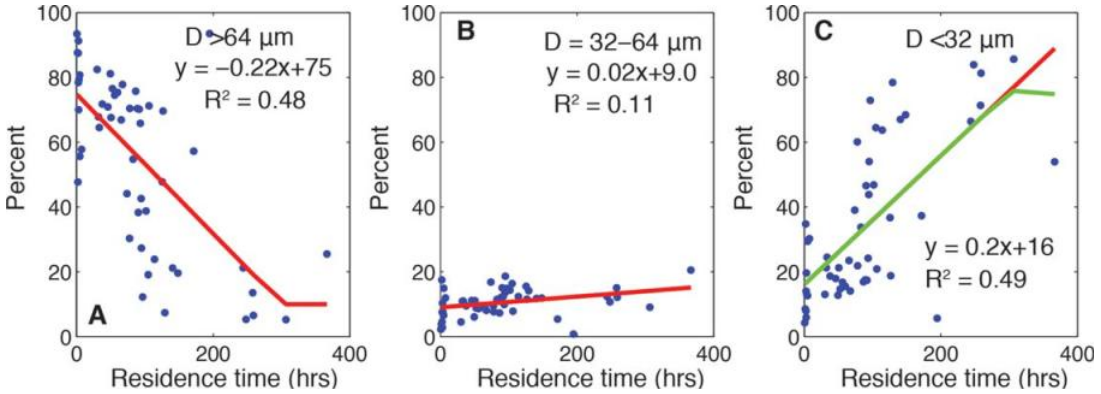


**Fig. 7.** Relationships between estimated residence times over the full model grid (Fig. 3a) and measured (a) sand, (b) coarse silt and (c) medium and finer silt and clay. The $>$ 64 $\mu$m was fit with a piecewise function, linear up to 300 h and constant 10% above 300 h. The 32–64 $\mu$m was fitted with a simple linear regression, whereas the $<$ 32 $\mu$m fraction was calculated as the remainder from 100% (green line in (c), which is not significantly different than a linear fit to measured values of the $<$ 32 $\mu$m fraction (red line in (c)). The relationships shown were used to create maps of these three grain-size fractions (e.g., Fig. 3b) from maps of residence time (Fig. 3a).

of SSC at the ADP site depended on the initial bed configuration, though values for both bed configurations have roughly the same correlation coefficient (0.55 for the uniform bed and 0.53 for and non-uniform bed) compared to the ADP-derived values. The initially uniform bed simulation overestimated SSC by an average of 10 mg/L while the initially non-uniform bed underestimated SSC by an average of 10 mg/L (Fig. 4e). SSC at the ADP site from the non-uniform bed simulations was most noticeably low early in the deployment period, but as the bed is reworked, estimates of SSC improved. In contrast SSC from the uniform bed simulations got worse over the period of the simulation (Fig. 4e). Both bed configurations captured the general timing of episodic resuspension events at the ADP site.

Pre- and post-simulation grain size distributions were compared to observed values along the sampling transects (Fig. 5). In general, sand fractions in the initially non-uniform bed changed little in sections of the transects where estimated and measured sand fractions were in good agreement (all of transect 3, fine end of transect 4, coarse end of transect 1). There was also little change in sand fraction from beginning to end of the initially uniform bed simulations in these regions, although the discrepancy between the uniform-bed sand fractions and measured sand fractions was much larger. Portions of transects with larger differences in pre- and post-simulation sand fractions tended to be sections where there was poor initial agreement between the non-uniform estimated and measured sand fractions. In transect 2, the model appears to have reworked the bed to more closely resemble the measured variation in sand fraction, with a decrease in sand fraction from 8 km to 14 km and an increase from 3 km to 8 km (Fig. 5). In contrast, reworking increased rather than decreased the difference between measured and simulated sand fractions in the 3–4 km stretch of transect 4 and increased the variability of sand fractions with relatively little change in mean sand fraction along the landward portion of transect 1.

### Spatial variations of SSC

Model simulations for the winter of 2002–2003 (Fig. 4) were used to examine the effect of the initially uniform vs. non-uniform bed sediment size distributions on spatial patterns of suspended sediment concentration (SSC; Fig. 8). To eliminate times when there was little to no sediment in suspension, means and standard deviations of SSC shown in Fig. 8 are for times when wind speed was in the upper quartile of winds for the 2002–2003 model period (wind speed $> 7.6$ m/s). This is close to the threshold wind speed of $\sim$ 7 m/s identified by Lawson et al. (2007) as necessary for significant resuspension in Hog Island Bay (Fig. 1), the large bay that extends from about 43–53 km on the vertical axis of the images in Fig. 8. Mean SSC in the range of 50–100 mg/L was widespread in the initially uniform bed case with comparable values of standard deviation. Notably, there were plumes of high SSC extending out of the inlets (regions that typically have high sand fractions) while SSC was relatively low adjacent to the mainland, where sediment is typically much finer. Mean SSC was more distinctly zonated for the initially non-uniform bed with lower values in the seaward portions of the bays and higher values in the landward portions with the standard deviation of SSC again following a similar pattern.

### Sensitivity of modeled suspended sediment concentrations

Modeled values of suspended sediment concentration (SSC) were most sensitive to the value assigned for the erosion parameter $M$, which is the least constrained of the model parameters. We set the value of $M$ to $1 \times 10^{-5}$ kg m$^{-2}$ s$^{-1}$ based on order of magnitude adjustments of $M$ in comparison to measured values of SSC at the ADP site in Hog Island Bay (Figs. 2a, 4). Locations most sensitive to the value of $M$ were those regions that are predominantly muddy, mostly in the more landward (western) portions of the bays. With $M = 1 \times 10^{-6}$ kg m$^{-2}$ s$^{-1}$, values of SSC dropped to near zero everywhere in the system. With $M = 1 \times 10^{-4}$ kg m$^{-2}$ s$^{-1}$, SSC values in some muddy regions of the bays reached 1000 mg/L, which is unrealistically high. It is worth noting, however, that these high values do not change the spatial patterns of SSC shown in Fig. 8, but rather amplify the differences in SSC between the sandier and muddier portions of the system. The value of $M = 1 \times 10^{-5}$ kg m$^{-2}$ s$^{-1}$ that we used in our calculations is consistent with previous modeling studies of coastal bays, such as San Francisco Bay where values of $M$ in the range of $1–5 \times 10^{-5}$ kg m$^{-2}$ s$^{-1}$ have been used (Ganju and Schoellhamer 2010; van der Wegen et al. 2011b).

Use of a modestly higher or lower representative settling velocity for the coarse silt and sand fractions had little effect on the results. Calculated SSC is more sensitive to the settling velocity assigned to the finer silt and clay fraction. As explained in the Methods, we assumed that the $< 32$ $\mu$m fraction settled as flocs with a representative floc settling rate of 0.75 mm/s. Varying this value affects the length of time that the fine fractions remain in the water column, but the volume of this fraction in suspension is primarily determined by the erosion parameter. Increasing active layer thickness from 5 cm to 10 cm and decreasing bed porosity from 0.7 to 0.5 resulted in small changes in SSC ($\leq$ 5 mg/L) in all except for a few very localized spots in the model domain.

## Discussion

### Spatial distribution of sediment properties

Analysis of bay bottom samples across four of the Virginia coastal bays (Figs. 5, 6) illustrates the strong grain size gradients that are often present in shallow coastal bays, with predominantly sandy sediment near tidal inlets and barrier islands and predominantly muddy sediment near the

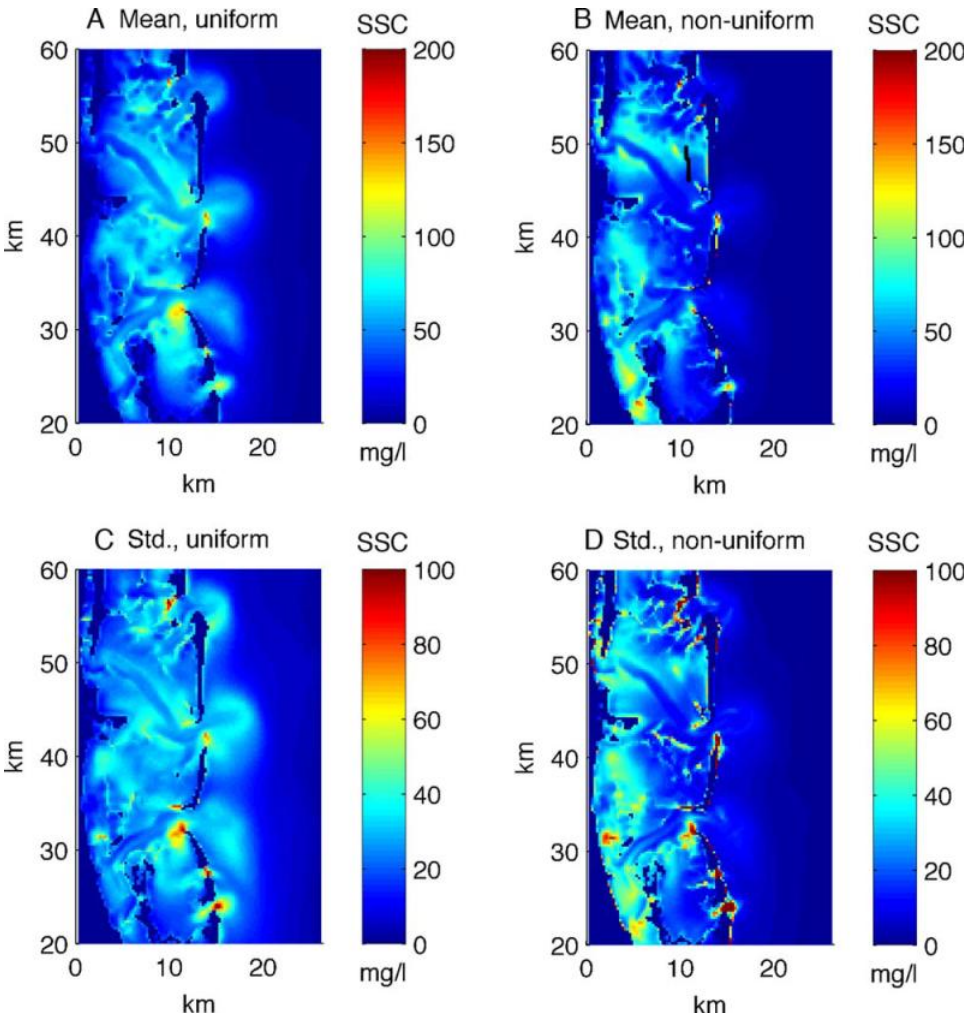


**Fig. 8.** Spatial patterns of means (a and b) and standard deviations (c and d) of suspended sediment concentrations when wind speed was in the upper quartile of values ($> 7.6$ m s$^{-1}$) during the 2-month simulation period in winter 2002–2003. Values for the initially uniform bed (a and c) and non-uniform bed (b and d) are shown for comparison.

mainland. This observation is not new, but it is hard to translate into maps of bay bottom sediment characteristics based on sampling alone. Bay bottom area in the Virginia Coast Reserve (VCR), for example, is extensive ($\sim$ 500 km$^2$) and assigning grain size and other sediment properties at a given location based on a limited number of in situ samples is a challenging problem. The relationships we found between residence time, which can be calculated using coastal circulation models, and grain size provide an objective approach for assigning bed sediment size fractions over all of the bays in our study area.

We found a strong inverse relationship between percent sand ($\geq$ 64 $\mu$m) and percent clay ($<$ 4 $\mu$m). We also found a strong negative relationship between sand fraction and organic matter (combustible) fraction, as expected based on the inverse relationship between particle surface area-to-volume ratio and particle diameter (Bergamaschi et al. 1997; Ganeshram et al. 1999). As a result of these relationships, a map of sand fractions (Fig. 3b) together with the relationships shown in Figs. 6 and 7 can be used as an indicator of a number of geomorphically, ecologically, and biogeochemically important bed characteristics including grain size distribution, organic content, permeability, and cohesive vs. noncohesive erosion behavior. For example, habitat requirements for benthic primary producers can be affected by a range of bed parameters including grain size, mobility, organic fraction and permeability (Koch 2001). Because high sand fractions are correlated with short residence times and relatively high flow speeds, these are also indicative of regions of rapid flushing, which can be important in terms of aquaculture operations and water quality concerns (Pratt and Campbell 1956; Grizzle et al. 1992).

Initializing a model with a spatially uniform distribution of sandy and muddy fractions and allowing those to evolve

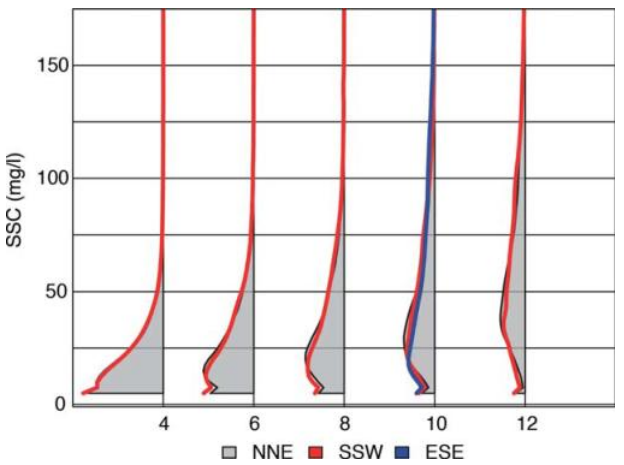


**Fig. 9.** Probability distributions of suspended sediment concentration (SSC) over the model domain for steady winds of 4 m $s^{-1}$, 6 m $s^{-1}$, 8 m $s^{-1}$, 10 m $s^{-1}$, and 12 m $s^{-1}$ blowing from the NNE (orientation of the long axis of system, gray shading), SSW (red curve) and ESE (orientation of short axis of system, blue curve for 10 m $s^{-1}$ winds only).

through time will also lead to bed coarsening (removal of fine sediment) in higher velocity zones near the inlets (Fig. 2b) and accumulation of finer sediment in the more distal, lower velocity regions of the model domain. There will also be export of fine sediment to the ocean. Significant exchange of water and particles with adjacent bays is limited to just a few of the Virginia coastal bays (Safak et al. 2015), suggesting that spatial redistribution of grain size fractions in model simulations using an initially uniform bed will tend to keep the mass of each size fraction relatively constant within each bay other than the sediment—mostly fine—lost to the ocean through inlet tidal exchange (plumes of high concentration in Fig. 8a). In contrast, we found that some bays have overall coarser than average beds while others have finer than average beds.

The extent of adjustment in sand fractions over the 2-month simulations, which represented a relatively windy period of time (Fig. 4), suggests that model simulations initialized with a uniform distribution of sediment will take a long time to internally redistribute sediment into a pattern resembling the natural distribution of sand and mud fractions in shallow coastal bays. It is possible to accelerate sediment redistribution through a morphologic factor in Delft3D model simulations (van der Wegen et al. 2011a), but not all coastal hydrodynamic models have this capability. While not perfect, the non-uniform distributions of sand and mud developed from calculated patterns of residence time capture the large-scale trends in measured grain size variations in the bays of the VCR, and can continue to adjust as simulations are run. Locations with large discrepancies in estimated vs. observed grain size, anomalously high calculated SSC, or rapid change in grain size distribution during model simulations are locations that likely merit scrutiny for potential measurement errors in depth and/or grain size or model grid errors. Potential depth errors in model grids are a particular concern as depths are often interpolated from scant measurements, can change over time, and affect modeled flow rates and hence estimated residence times as well as sediment erosion and deposition.

### Spatial patterns of SSC

Calculated spatial distributions of SSC during resuspension conditions strongly reflected spatial variations in bed sediment size in model simulations. Large portions of the bays had mean SSC in the range of 50–100 mg/L for the initially uniform bed simulations when wind speeds were in the upper quartile of their distribution ($> 7.6$ m/s) owing to the ubiquitous presence of fine sediment in the bay bottoms. In contrast, for the same wind conditions there were distinct regions of higher and lower SSC in the initially non-uniform bed simulations, which corresponded to regions of low and high sand fraction (Fig. 3b), respectively. The one region where SSC was notably higher in the initially non-uniform bed runs is close to the mainland. For both the uniform and non-uniform beds, spatial distributions of the standard deviations of SSC were similar to spatial distribution of mean SSC. This is not surprising in a system in which SSC is at low levels for a large fraction of the time such that regions with episodically high mean SSC are also regions with the most variable SSC.

The winter 2002–2003 simulations provide insight into natural temporal and spatial variability in SSC, but it is hard to get a sense of the relative importance of different wind speeds and directions in determining the overall response. To investigate this, we ran the non-uniform bed model for a set of constant wind speeds (4 m $s^{-1}$, 6 m $s^{-1}$, 8 m $s^{-1}$, 10 m $s^{-1}$, and 12 m $s^{-1}$) and several wind directions. The dominant wind directions in the VCR are along the axis of the Delmarva Peninsula (Fig. 1), with the highest winds from the NNE and the most frequent winds from the SSW (Fagherazzi and Wiberg 2009; McLoughlin et al. 2015). Winds from these two directions were run for the five constant wind speeds. In addition, we ran one case (wind speed of 10 m/s) with onshore winds (from the ESE) to see how much that affected SSC.

At low wind speeds ($\leq$ 6 m $s^{-1}$), SSC was near zero over large regions of the bays and modal values were $< 15$ mg $L^{-1}$ (Fig. 9). As wind speed increased, mean and modal values of SSC increased and the high SSC tails of the distributions become increasingly elongated. By a wind speed of 10 m $s^{-1}$, very little of the bay bottoms had near-zero SSC. Winds from the NNE generated slightly higher SSC than those from the SSW, but the distributions were quite similar (Fig. 9). Winds from ESE (across the peninsula) resulted in smaller average SSC compared to winds along the peninsula (Fig. 9, green curve for wind speed = 10 m $s^{-1}$), likely owing to smaller average fetch, but they were still capable of producing

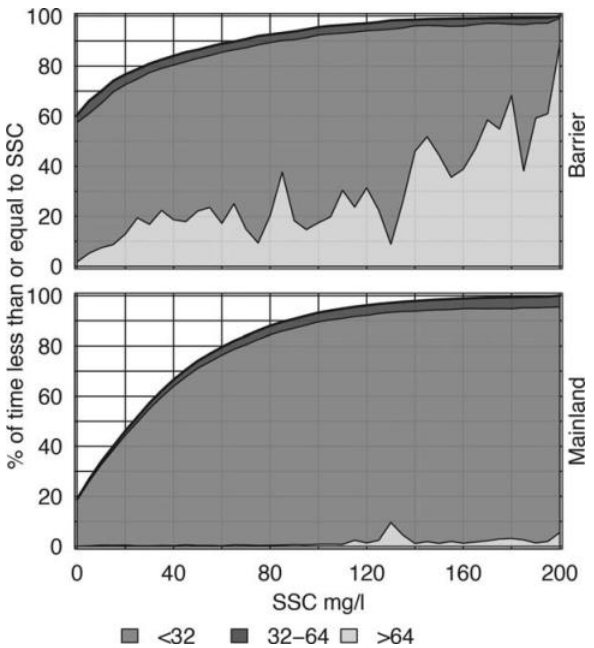


**Fig. 10.** Cumulative distribution of simulated values of suspended sediment concentration (SSC) at sites close to (a) back-barrier marshes and (b) close to mainland marshes. The colors indicate the grain size distribution in the water column for each value of SSC.

localized regions of high SSC. These results are consistent with several field-based studies (Lawson et al. 2007; Duvall 2014) that have shown that wind speeds $> 7$ m $s^{-1}$ are required for significant increases in SSC in Hog Island Bay, the large central bay in the VCR (Fig. 1).

### Impact of spatially varying SSC on marsh deposition and benthic plants

Spatiotemporal patterns of SSC are likely to play a role in the ability of salt marshes to withstand relative sea-level rise. Salt marshes are vulnerable to sea-level rise if the rate at which marsh surface elevation increases is not able to keep up with changes in sea level through a combination of inorganic sediment deposition and organic matter accumulation. A number of studies have explored the vulnerability of marshes to sea-level rise (Allen 1990; van Wijnen and Bakker 2001; Morris et al. 2002; French 2006; Kirwan et al. 2010; Mariotti and Fagherazzi 2010, 2013; D'Alpaos et al. 2011; Mariotti and Carr 2014). For example, Kirwan et al. (2010) combined the results of a number of marsh models to define threshold rates of sea-level rise leading to marsh collapse as a function of SSC and tidal range, where SSC served as a measure of sediment availability for deposition on the marsh surface. The higher the representative SSC in a location, the larger the rate of relative sea-level rise it can withstand all else being equal.

Models of the long-term response of a salt marsh to sea-level rise generally use a single, constant value of SSC to represent the allochthonous sediment supply to a marsh (Kirwan et al. 2010). Estimates of SSC in coastal environments, like those of bed sediment characteristics, tend to be based on relatively little data. In situ sampling of SSC is often limited to relatively calm conditions. Sensors that measure optical or acoustic backscatter from particles in suspension allow for longer duration sampling and are often combined with hydrodynamic measurements to more fully characterize resuspension and transport processes in coastal environments (e.g., Voulgaris and Meyers 2004; Lawson et al. 2007; Mariotti et al. 2010), but are limited to a few sites. Model simulations such as those presented in this study offer the opportunity to assess spatial and temporal variability of SSC and its implications for sediment supply to marshes.

Spatial distributions of average SSC for the initially non-uniform bed during moderate—high wind conditions (Fig. 8b) reveal strong variations in SSC across the bays. Whereas the landward portions of the bays are generally characterized by relatively high SSC, values near the islands are generally much lower, suggesting that tidal flooding has the potential to supply more sediment to mainland marshes than back-barrier marshes. To quantify this difference, we identified model grid cells that fronted open water, had elevations below mean sea level, and were within 500 m (two grid cells) of back-barrier and mainland marshes in Hog Island Bay.

The cumulative distribution function of SSC near the back-barrier marshes indicates that relatively low turbidity was predominant at these sites (Fig. 10a). For example, SSC $< 50$ mg $L^{-1}$ (a representative concentration used by Kirwan et al. (2010) for a mainland marsh in the VCR) more than 85% of the time during the winter 2002–2003 simulations at the back-barrier sites. Since winter tends to be the stormier season, this is likely to be true for the rest of the year as well. There was an increasing trend of percentage sand in suspension with increasing SSC near the back-barrier marshes (Fig. 10a). Owing to its higher settling velocity, sand is less likely than the mud to be well mixed through the water column during high water conditions (high spring tides or storm surge). Because only the sediment suspended in the upper portion of the water column has the potential to be transported onto the marsh surface, higher SSC does not necessarily translate into a proportional increase in sediment supply to the back-barrier marshes. It is worth noting, however, that back-barrier marshes have an alternative source of sediment from overwash that may be important for maintenance of marsh elevation as sea level rises (Walters et al. 2014).

The cumulative distribution function of SSC near the mainland marshes was higher than near the back-barrier marshes and was almost totally lacking in sand, even at high SSC (Fig. 10b). SSC exceeded 50 mg $L^{-1}$ about 25% of time during the winter 2002–2003 simulation with an initially non-uniform bed. The differences between SSC near the

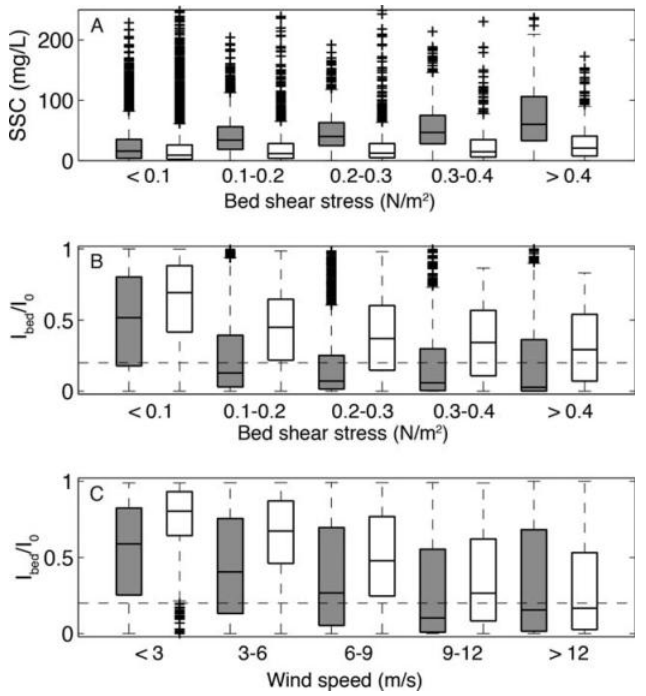


**Fig. 11.** (a) Box plots of suspended sediment concentration (SSC) as a function of bed shear stress for sites with depths in the range of 0.6–1.6 m near back-barrier marshes (unfilled boxes) and mainland marshes (boxes filled in gray). (b) Box plots of percent incident light ($I_0$) reaching the bay bottom as a function of bed shear stress for the same sites as in (a). (c) Box plots showing the same data as in (b) but binned according to wind speed. The horizontal dashed lines in (b) and (c) indicate the 20% incident radiation condition that has been suggested as a requirement for seagrass growth.

mainland and back-barrier marshes were more pronounced for lower SSC. For example, near the mainland marsh SSC $>20$ mg $L^{-1}$ for more than half of the simulation whereas this was true near the back-barrier marshes less than 25% of the time. How best to relate short-term measured or modeled near-marsh SSC to long-term sediment supply to marshes remains an open question.

Water column turbidity reduces the light available for photosynthesis by benthic plants. In the Virginia coastal bays, suspended sediment is the primary control on turbidity, as algal concentrations in the water column and other contributors to turbidity (Gallegos 2001) are low (Lawson et al. 2007; McGlathery et al. 2009). As a consequence, spatial patterns of SSC, together with water depth, determine the spatial distribution of benthic light availability (Lawson et al. 2007). To detail the potential impacts of spatial variations in bed properties on light reaching the bay bottom, we selected sites from the previously discussed set of sites near mainland and back-barrier marshes that fell within a depth range of 0.6–1.6 m. The shallower limit corresponds to mean low water while the deeper limit is the maximum observed depth for seagrass in the VCR (McGlathery et al. 2012). Comparison of SSC near the mainland and back-barrier regions of the system for equivalent ranges of bed shear stress (Fig. 11a) indicates that above a bed shear stress of 0.1 N $m^{-2}$, SSC at the muddier sites near the mainland was consistently higher than SSC at the sandier sites near the barrier islands. Bed shear stress for both sets of sites was $>0.1$ N $m^{-2}$ about 25% of the time during our winter 2002–2003 simulation.

We used the Lambert-Beer Law, $I/I_0 = e^{-Kz}$, to estimate light attenuation at the bay bottom (Fig. 11b), where $K$ is the light attenuation coefficient, $z$ is water depth and $I/I_0$ is fraction of incident light. Light attenuation coefficients in coastal bays, typically taken to be the downwelling light attenuation coefficient $K_d$, are site specific (Gallegos 2001). Based on the results of Lawson et al. (2007) for Hog Island Bay (Fig. 1), $K_d \approx 0.052 \times \mathrm{SSC} + 0.24$ $m^{-1}$ for typical (and relatively constant) values of chlorophyll $a$ and dissolved organics. Seagrass has been estimated to require about 20% incident radiation for growth (Duarte 1991). When bed shear stresses were $>0.1$ N $m^{-2}$, calculated light reaching the bay bottom at the mainland sites was most often $<20\%$ of incident light whereas light reaching the bay bottom at the back-barrier sites was mostly $>20\%$ of incident light even at the highest bed shear stresses.

The most relevant light conditions for seagrass are those that occur during spring and summer, when seagrass is most productive. Tidal conditions in spring-summer are the same as in winter, but winds are more moderate. For example, from November 2002 to January 2003, which extends through the period of our simulations, winds were $\leq 6$ m $s^{-1}$ 60% of the time and $>9$ m $s^{-1}$ 15% of the time. In comparison, winds were $\leq 6$ m $s^{-1}$ 80% of the time and $>9$ m $s^{-1}$ just 3% of the time from May to July 2003. If we recast light attenuation at the mainland and back-barrier sites in terms of wind speed (Fig. 11c), we find that in almost all cases, $>20\%$ of incident light reached the bay bottoms at the back-barrier sites when wind speed $\leq 6$ m $s^{-1}$ and that even at higher speeds of 6–9 m $s^{-1}$, the fraction of incident light at the bed exceeded 20% for more than 75% of the record. This suggests that light is seldom limiting for seagrass in the sandier, back-barrier regions of the bays, consistent with the success of seagrass restoration efforts in sandier regions of several bays in the VCR (McGlathery et al. 2012). For the muddier mainland sites, light conditions for low winds ($\leq 3$ m $s^{-1}$) were similar to those for moderate winds (6–9 m $s^{-1}$) at the back-barrier sites. The availability of adequate light for seagrass growth in the muddier regions of the bay is therefore likely to be more sensitive to the windiness of the growing season, with the possibility of light limitation in these regions during windier-than-normal spring—summer time periods.

These simulations do not include the effects of seagrass on flow or SSC, which are known to increase water clarity (de Boer 2007; van der Heide et al. 2007; Carniello et al. 2014). Because the light environment in sandier regions of

the bays is adequate for survival seagrass in the absence of a full meadow, new shoots should not experience significant light limitation at depths $\leq 1.6$ m (Fig. 11c). As these develop into meadows, the light environment will continue to improve. In muddier regions of the bays, light may limit the establishment of new shoots (Fig. 11c). In addition, the relationship used here for light attenuation was developed for a site in the sandier part of Hog Island Bay (ADP site in Fig. 2a). Light attenuation in the water column increases with decreasing suspended particle size for any given value of SSC (Wiberg et al. 1994). Because a larger fraction of the sediment in suspension at the mainland sites is in the finest size class compared to the back-barrier sites, we likely underestimate light attenuation in these muddy portions of the bays. This suggests that the probability of successful establishment of seagrass shoots and meadows is much smaller in the muddier regions of the bays near the mainland compared to the sandier, seaward portions of the bays.

**Comments and recommendations**

One of the strengths of the proposed approach combining residence time calculations with sediment sampling to estimate spatial patterns of grain size fractions in shallow bays is that it requires neither extensive dedicated modeling nor extensive sampling. If the purpose of developing the grain size maps is to improve simulations of sediment resuspension and transport, then implementation of a hydrodynamic model will already be part of the project. The results of Safak et al. (2015) suggest that a 2-month-long simulation that includes tracking of neutrally buoyant particles is sufficient to capture the main spatial patterns of residence time. However, particle tracking may not be necessary. Shortest path residence times (SPRT) can be calculated simply from RMS velocity and distance to the nearest inlet for each subtidal point in a model domain. Even though SPRT is not a good representation of actual residence time outside of the tidally refreshed zone near the inlets, the relationship between SPRT and particle-tracking residence time (PTRT) is sufficiently linear that a regression between SPRT and percent sand ($R^2 = 0.49$, $p < 0.05$) is nearly as strong as that between PTRT and percent sand ($R^2 = 0.55$; Fig. 6).

Maps of the distribution of residence times can be used to target sediment sampling to capture the end members plus a limited set of transitional sites from which to build the relationships between residence time and sediment size fractions. In the Virginia Coast Reserve (VCR), one set of relationships was adequate to characterize the residence-time vs. size fraction relationships for all of the bays we sampled (Fig. 6). However, this may not be true for all systems.

In systems lacking external sediment sources, such as the VCR, internally supplied sediment, e.g., from marsh edge erosion, appears to be quickly reworked (e.g., McLoughlin et al. 2015) so that bed properties are generally in equilibrium with the flow conditions. In systems with a significant sediment source, such as a river discharging sediment into the system during seasonal flooding, sediment will be introduced at the muddier, landward margin of the system but may disperse more broadly, maintaining a larger fraction of fine sediment than otherwise expected in regions with relatively short residence times. The same hydrodynamic model used to estimate flow and residence times could be used to estimate a dispersal footprint for sediment delivered to the system during floods. It may be possible to add this to the background pattern derived from residence time alone to develop more accurate grain size maps for systems with external sediment sources. The presence of a significant external source of sediment could also complicate the relationship between residence time and size fractions if, e.g., sampling transects cross a zone of flood deposition. Information about the extent of the depositional footprint from other sampling (e.g., Be-7) or modeling would be useful in identifying appropriate sampling sites.

## Conclusions

Knowledge of bed properties is important for geomorphological, ecological and biogeochemical analysis and modeling in shallow coastal bays but seldom are these properties mapped at the spatial resolution needed for these efforts. We have developed a method for mapping sediment size fractions and associated properties (e.g., organic fraction) that can build on results from circulation modeling and analysis of bed properties that may already have been done for a coastal bay or system of bays with limited additional effort. The effort is more significant in bays that have not been the target of a coastal circulation model, but, increasingly, some degree of hydrodynamic modeling is a component of studies of coastal bays. Our results suggest that flow calculations together with analysis of a limited number of strategically sited bed samples is sufficient to develop useful maps of grain size fractions and related bed properties in shallow bays.

Modeling of spatial patterns of suspended sediment concentration (SSC) based on the non-uniform distributions we obtained for sandy and muddy bed fractions demonstrates that SSC, and therefore turbidity and light attenuation, are strongly linked to the spatial distribution of bed sediment fractions. This is not surprising, but our results also show that quantifying spatial variations in SSC is challenging in the absence of spatial knowledge of bed sediment properties. Resolving SSC spatially is useful for understanding spatial variations in the distribution of benthic primary producers and for guiding efforts to restore habitat such as seagrass meadows (McGlathery et al. 2012). Knowledge of spatiotemporal variations in SSC is also important for quantifying sediment supplies for marsh deposition, a critical determinant of marsh vulnerability to sea-level rise. We found that spatial variations in bed sediment properties across coastal bays

translate into lower values of SSC adjacent to back-barrier marshes compared to mainland fringing marshes that may be important to account for in studies of marsh vulnerability to sea-level rise.

## References


Allen, J. R. L. 1990. Salt-marsh growth and stratification: A numerical model with special reference to the Severn Estuary, southwest Britain. Mar. Geol. **95**: 77–96. doi:10.1016/0025-3227(90)90042-I

Allen, T. R., G. F. Oertel, and G. McLeod. 2011. Synoptic assessment of repletion and residual water dynamics in a coastal lagoon by thermal remote sensing: Great Machipongo Lagoon (Hog Island Bay), Virginia, USA. IEEE J. Select. Topic Appl. Earth Obs. Remote Sens. **4**: 147–158. doi:10.1109/JSTARS.2010.2070488

Bergamaschi, B. A., E. Tsamakis, R. G. Keil, G. Eglinton, D. B. Montlucon, and J. I. Hedges. 1997. The effect of grain size and surface area on organic matter, lignin and carbohydrate concentration, and molecular compositions in Peru Margin sediments. Geochim. Cosmochim. Acta **61**: 1247–1260. doi:10.1016/S0016-7037(96)00394-8

Booij, N., R. C. Ris, and L. H. Holthuijsen. 1999. A third-generation wave model for coastal regions. 1. Model description and validation. J. Geophys. Res.: Oceans **104**: 7649–7666. doi:10.1029/98JC02622

Carniello, L., A. Defina, and L. D'Alpaos. 2012. Modeling sand-mud transport induced by tidal currents and wind waves in shallow microtidal basins: Application to the Venice Lagoon (Italy). Estuar. Coast. Shelf Sci. **102–103**: 105–115. doi:10.1016/j.ecss.2012.03.016

Carniello, L., S. Silvestri, M. Marani, A. D'Alpaos, A. Volpe, and A. Defina. 2014. Sediment dynamics in shallow tidal basins: In situ observations, satellite retrievals, and numerical modeling in the Venice Lagoon. J. Geophys. Res.: Earth Surf. **119**: 802–815. doi:10.1002/2013JF003015

Carr, J., P. D'Odorico, K. J. McGlathery, and P. L. Wiberg. 2010. Stability and bistability of seagrass ecosystems in shallow coastal lagoons: Role of feedbacks with sediment resuspension and light attenuation. J. Geophys. Res.: Biogeosci. **115**: G03011. doi:10.1029/2009JG001103

Castillo, E., R. Pereda, J. M. de Luis, R. Medina, and J. Viguri. 2011. Sediment grain size estimation using airborne remote sensing, field sampling, and robust statistic. Environ. Monit. Assess. **181**: 431–444. doi:10.1007/s10661-010-1839-z

Chen, C., R. C. Beardsley, and G. W. Cowles. 2006. An unstructured grid, finite-volume coastal ocean model (FVCOM) system. Oceanography **19**: 78–89. doi:10.5670/oceanog.2006.92

Christiansen, T., P. L. Wiberg, and T. G. Milligan. 2000. Flow and sediment transport on a tidal salt marsh surface. Estuar. Coast. Shelf Sci. **50**: 315–331. doi:10.1006/ecss.2000.0548

D'Alpaos, A., S. M. Mudd, and L. Carniello. 2011. Dynamic response of marshes to perturbations in suspended sediment concentrations and rates of relative sea level rise. J. Geophys. Res.: Earth Surf. **116**: F04020. doi:10.1029/2011JF002093

de Boer, W. F. 2007. Seagrass-sediment interactions, positive feedbacks and critical thresholds for occurrence: A review. Hydrobiologia **591**: 5–24. doi:10.1007/s10750-007-0780-9

Duarte, C. M. 1991. Seagrass depth limits. Aquat. Bot. **7**: 139–150. doi:10.1016/0304-3770(91)90081-F

Duvall, M. S. 2014. The effects of waves and tidal inundation on sediment deposition and flux across a bay-marsh boundary. M.S. thesis. Univ. of Virginia.

Fagherazzi, S., and P. L. Wiberg. 2009. Controls on fetch, wind waves and wave-generated shear stresses in a shallow coastal lagoon. J. Geophys. Res.: Earth Surf. **114**: F03022. doi:10.1029/2008JF001139

Fagherazzi, S., G. Mariotti, A. T. Banks, E. J. Morgan, and R. W. Fulweiler. 2014. The relationships among hydrodynamics, sediment distribution, and chlorophyll in a mesotidal estuary. Estuar. Coast. Shelf Sci. **144**: 54–64. doi:10.1016/j.ecss.2014.04.003

Fonseca, M. S., and S. S. Bell. 1998. Influence of physical setting on seagrass landscapes near Beaufort, North Carolina, USA. Mar. Ecol. Prog. Ser. **171**: 109–121. doi:10.3354/meps171109

French, J. 2006. Tidal marsh sedimentation and resilience to environmental change: Exploratory modelling of tidal, sea-level and sediment supply forcing in predominantly allochthonous systems. Mar. Geol. **235**: 119–136. doi:10.1016/j.margeo.2006.10.009

French, J. R., and T. Spencer. 1993. Dynamics of sedimentation in a tide-dominated backbarrier salt-marsh, Norfolk, UK. Mar. Geol. **110**: 315–331. doi:10.1016/0025-3227(93)90091-9

Fugate, D. C., C. T. Friedrichs, and A. Bilgili. 2006. Estimation of residence time in a shallow back barrier lagoon, Hog Island Bay, Virginia, USA. *In* M. Spaulding [ed.], 9th International Conference on Estuarine and Coastal Modeling. Charleston, SC.

Furukawa, K., E. Wolanski, and H. Mueller. 1997. Currents and sediment transport in mangrove forests. Estuar. Coast. Shelf Sci. **44**: 301–310. doi:10.1006/ecss.1996.0120

Gallegos, C. L. 1994. Refining habitat requirements of submersed aquatic vegetation—role of optical models. Estuaries **17**: 187–199.

Gallegos, C. L. 2001. Calculating optical water quality targets to restore and protect submersed aquatic vegetation: Overcoming problems in partitioning the diffuse attenuation coefficient for photosynthetically active radiation. Estuaries **24**: 381–397. doi:10.2307/1353240

Ganeshram, R. S., S. E. Calvert, T. F. Pedersen, and G. L. Cowie. 1999. Factors controlling the burial of organic carbon in laminated and bioturbated sediments off NW Mexico:

Implications for hydrocarbon preservation. Geochim. Cosmochim. Acta **63**: 1723–1734. doi:10.1016/S0016-7037(99)00073-3

Ganju, N. K., and D. H. Schoellhamer. 2010. Decadal-timescale estuarine geomorphic change under future scenarios of climate and sediment supply. Estuaries Coasts **33**: 15–29. doi:10.1007/s12237-009-9244-y

Giordano, J. P., M. J. Brush, and I. C. Anderson. 2011. Quantifying annual nitrogen loads to Virginia's coastal lagoons: Sources and water quality response. Estuaries Coasts **34**: 297–309. doi:10.1007/s12237-010-9345-7

Grizzle, R. E., R. Langan, and W. H. Howell. 1992. Growth responses of suspension-feeding bivalve molluscs to changes in water flow: Differences between siphonate and nonsiphonate taxa. J. Exp. Mar. Biol. Ecol. **162**: 213–228. doi:10.1016/0022-0981(92)90202-L

Hansen, J. C. R., and M. A. Reidenbach. 2012. Wave and tidally driven flows in eelgrass beds and their effect on sediment suspension. Mar. Ecol. Prog. Ser. **448**: 271–287. doi:10.3354/meps09225

Hill, P. S., J. P. Newgard, B. A. Law, and T. G. Milligan. 2013. Flocculation on a muddy intertidal flat in Willapa Bay, Washington, Part II: Observations of suspended particle size in a secondary channel and adjacent flat. Cont. Shelf Res. **60**: S145–S156. doi:10.1016/j.csr.2012.06.006

Khelifa, A., and P. S. Hill. 2006. Models for effective density and settling velocity of flocs. J. Hydraul. Res. **44**: 390–401. doi:10.1080/00221686.2006.9521690

Kirwan, M. L., G. R. Guntenspergen, A. D'Alpaos, J. T. Morris, S. M. Mudd, and S. Temmerman. 2010. Limits on the adaptability of coastal marshes to rising sea level. Geophys. Res. Lett. **37**: L23401. doi:10.1029/2010GL045489

Koch, E. M. 2001. Beyond light: Physical, geological, and geochemical parameters as possible submersed aquatic vegetation habitat requirements. Estuaries **24**: 1–17. doi:10.2307/1352808

Law, B. A., T. G. Milligan, P. S. Hill, J. Newgard, R. A. Wheatcroft, and P. L. Wiberg. 2013. Flocculation on a muddy intertidal flat in Willapa Bay, Washington, Part I: A regional survey of the grain size of surficial sediments. Cont. Shelf Res. **60**: S136–S144. doi:10.1016/j.csr.2012.06.007

Lawson, S. E., P. L. Wiberg, K. J. McGlathery, and D. C. Fugate. 2007. Wind-driven sediment suspension controls light availability in a shallow coastal lagoon. Estuaries Coasts **30**: 102–112. doi:10.1007/BF02782971

Mariotti, G., and S. Fagherazzi. 2010. A numerical model for the coupled long-term evolution of salt marshes and tidal flats. J. Geophys. Res.: Earth Surf. **115**: F01004. doi:10.1029/2009JF001326

Mariotti, G., S. Fagherazzi, P. L. Wiberg, K. J. McGlathery, L. Carniello, and A. Defina. 2010. Influence of storm surges and sea level on shallow tidal basin erosive processes. J. Geophys. Res.: Oceans **115**: C11012. doi:10.1029/2009JC005892

Mariotti, G., and S. Fagherazzi. 2013. Critical width of tidal flats triggers marsh collapse in the absence of sea-level rise. Proc. Natl. Acad. Sci. USA **110**: 5353–5356. doi:10.1073/pnas.1219600110

Mariotti, G., and J. A. Carr. 2014. Dual role of salt marsh retreat: Long-term loss and short-term resilience. Water Res. Res. **50**: 2963–2974. doi:10.1002/2013WR014676

McGlathery, K., P. Wiberg, R. Christian, and L. Blum. 2009. Integrated Water Quality Data Spreadsheets for lagoons of the Virginia Coast Reserve 1992–2008. Virginia Coast Reserve Long-Term Ecological Research Project Data Publication knb-lter-vcr.178.14. Available from http://metacat.lternet.edu/knb/metacat/knb-lter-vcr.178.14/lter

McGlathery, K. J., L. Reynolds, L. W. Cole, R. J. Orth, and A. Schwarzchild. 2012. Recovery trajectories during state change from bare sediment to eelgrass dominance. Mar. Ecol. Prog. Ser. **448**: 290–221. doi:10.3354/meps09574

McLoughlin, S. M., P. L. Wiberg, I. Safak, and K. J. McGlathery. 2015. Rates and forcing of marsh edge erosion in a shallow coastal bay. Estuaries Coasts **38**: 620–638. doi:10.1007/s12237-014-9841-2

Morris, J. T., P. V. Sundareshwar, C. T. Nietch, B. Kjerfve, and D. R. Cahoon. 2002. Responses of coastal wetlands to rising sea level. Ecology **83**: 2869–2877. doi:10.2307/3072022

Olson, M. S., J. S. Herman, A. C. Sofranko, and A. L. Mills. 2006. Nitrate loading as a function of stream discharge along the Eastern Shore of Virginia. Annual Meeting, Geological Society of America, Philadelphia, PA.

Orth, R. J., M. L. Luckenbach, S. R. Marion, K. A. Moore, and D. J. Wilcox. 2006. Seagrass recovery in the Delmarva Coastal Bays, USA. Aquat. Bot. **84**: 26–36. doi:10.1016/j.aquabot.2005.07.007

Partheniades, E. 1965. Erosion and deposition of cohesive soils. J. Hydraul. Div. Am. Soc. Civ. Eng. **91**: 105–139.

Pratt, D. M., and D. A. Campbell. 1956. Environmental factors affecting growth in *Venus mercenaria*. Limnol. Oceanogr. **1**: 2–17. doi:10.4319/lo.1956.1.1.0002

Richardson, D., J. Porter, G. Oertel, R. Zimmerman, C. Carlson, and K. Overman. 2014. Integrated topography and bathymetry for the eastern shore of Virginia. Long Term Ecological Research Network. Available from http://dx.doi.org/10.6073/pasta/ff26e33c1cf34ab11d55efaf3569d0e6

Roelvink, J. A. 2006. Coastal morphodynamic evolution techniques. Coast. Eng. **53**: 177–187. doi:10.1016/j.coastaleng.2005.10.015

Roelvink, J. A., and G. K. F. M. Van Banning. 1994. Design and development of DELFT3D an application to coastal morphodynamics, p. 451–456. *In* Proceedings of International Conference on Hydroinformatics 1994, Delft, The Netherlands.

Safak, I., and P. L. Wiberg. 2012. Hydrodynamics and wave-enhanced sediment transport in a barrier island-lagoon-marsh system: A model application on the Eastern Shore

of Virginia. Abstract 029-9350, 2012 Ocean Sciences Meeting, American Geophysical Union, Salt Lake City, UT.

Safak, I., P. L. Wiberg, D. L. Richardson, and M. O. Kurum. 2015. Controls on residence time and exchange in a system of shallow coastal bays. Cont. Shelf Res. **97**: 7–20. doi:10.1016/j.csr.2015.01.009

van der Heide, T., E. H. van Nes, G. W. Geerling, A. J. P. Smolders, T. J. Bouma, and M. M. van Katwijk. 2007. Positive feedbacks in seagrass ecosystems: Implications for success in conservation and restoration. Ecosystems **10**: 1311–1322. doi:10.1007/s10021-007-9099-7

van der Wal, D., and P. M. J. Herman. 2007. Regression based synergy of optical, shortwave infrared and microwave remote sensing for monitoring the grain-size of intertidal sediments. Remote Sens. Environ. **111**: 89–106. doi:10.1016/j.rse.2007.03.019

van der Wegen, M., and J. A. Roelvink. 2008. Long-term morphodynamic evolution of a tidal embayment using a two-dimensional, process-based model. J. Geophys. Res.: Oceans **113**: C03016. doi:10.1029/2006JC003983

van der Wegen, M., B. E. Jaffe, and J. A. Roelvink. 2011a. Process-based, morphodynamic hindcast of decadal deposition patterns in San Pablo Bay, California, 1856–1887. J. Geophys. Res.: Earth Surf. **116**: F02008. doi:10.1029/2009JF001614

van der Wegen, M., A. Dastgheib, B. E. Jaffe, and J. A. Roelvink. 2011b. Bed composition generation for morphodynamic modeling: Case study of San Pablo Bay in California, U.S.A. Ocean Dyn. **61**: 173–186. doi:10.1007/s10236-010-0314-2

van Ledden, M., W. G. M. van Kestern, and J. C. Winterwerp. 2004. A conceptual framework for the erosion behaviour of sand-mud mixtures. Cont. Shelf Res. **24**: 1–11. doi:10.1016/j.csr.2003.09.002

van Rijn, L. C. 1993. *Principles of sediment transport in rivers, estuaries and coastal seas*. Aqua Publications.

van Rijn, L. C., J. A. Roelvink, and W. T. Horst. 2001. Approximation formulae for sand transport by currents and waves and implementation in DELFT-MOR. Tech. Rep. Z3054.40, WL Delft Hydraulics, Delft, The Netherlands.

van Wijnen, H. J., and J. P. Bakker. 2001. Long-term surface elevation change in salt marshes: A prediction of marsh response to future sea-level rise. Estuar. Coast. Shelf Sci. **52**: 381–390. doi:10.1006/ecss.2000.0744

Venier, C., A. D'Alpaos, and M. Marani. 2014. Evaluation of sediment properties using wind and turbidity observations in the shallow tidal areas of the Venice Lagoon. J. Geophys. Res.: Earth Surf. **119**: 1604–1616. doi:10.1002/2013JF003019

Voulgaris, G., and S. T. Meyers. 2004. Temporal variability of hydrodynamics, sediment concentration and sediment settling velocity in a tidal creek. Cont. Shelf Res. **24**: 1659–1683. doi:10.1016/j.csr.2004.05.006

Walters, D., L. J. Moore, O. Duran Vinent, S. Fagherazzi, and G. Mariotti. 2014. Interactions between barrier islands and backbarrier marshes affect island system response to sea level rise: Insights from a coupled model. J. Geophys. Res.: Earth Surf. **119**: 2013–2031. doi:10.1002/2014JF003091

Wiberg, P. L., D. E. Drake, and D. A. Cacchione. 1994. Sediment resuspension and bed armoring during high bottom stress events on the northern California inner continental shelf: Measurements and predictions. Cont. Shelf Res. **14**: 1191–1220. doi:10.1016/0278-4343(94)90034-5

## Acknowledgments

We thank Karen McGlathery and an anonymous reviewer for valuable suggestions that improved the manuscript. We also thank David Richardson and John Porter for assistance with generating the model grid and map figures. The developers of Delft3D are acknowledged for open access to their code. This research was supported by Office of Naval Research Grant N00014-13-10149 with additional funding from National Science Foundation Grant DEB-1237733 and the College and Graduate School of Arts and Sciences at the University of Virginia.

*Submitted 26 February 2015*
*Revised 25 June 2015*
*Accepted 13 August 2015*

*Associate editor: John Crimaldi*